High frequency impedance spectra of soft amorphous fibers

D. Ménard, M. Britel, P. Ciureanu, and A. Yelon
Groupe de Recherche en Physique et Technologie de Couches Minces and Department of Engineering Physics, Ecole Polytechnique, P. O. Box 6079, Station ''Centre-ville'', Montreal, Quebec, H3C 3A7, Canada

V. P. Paramonov and A. S. Antonov
Russian Academy of Science, SCAPE, IVTAN, Izhorskaya 13/19, Moscow 127412, Russia

P. Rudkowski and J. O. Ström-Olsen
Physics Department, McGill University, 3600 University, Montreal, Quebec, H3A 2T8, Canada

Giant magnetoimpedance (GMI) spectra of soft amorphous magnetic fibers, measured in the 1 kHz–1.2 GHz frequency range, and GMI responses, measured in the field range of ±120 Oe, have reinforced the assumption that linear giant magnetoimpedance and ferromagnetic resonance (FMR) have the same physical origin. The samples, NiCo-rich, CoFe-rich, and Metglas-type fibers, 30–40 μm in diameter, were cast by melt extraction. Their impedance has been measured up to 13 MHz, in the presence of a magnetic field, using an impedance analyzer. These measurements have been extended up to 1.2 GHz by using a network analyzer. The reflection coefficient of a shorted coaxial line whose inner conductor was replaced by a magnetic fiber was measured, and the input impedance per unit length of this line was then calculated. The two impedances above are equivalent and their spectra show a behavior associated with FMR: the real part of the impedance peaks at a frequency where the imaginary part passes through zero. [S0021-8979(97)21808-6]

It is generally agreed that the giant magnetoimpedance (GMI) effect in soft magnetic materials originates from the dependence of the skin depth upon the magnetic permeability, which changes substantially when an external magnetic field is applied. Although several recent publications have discussed the origins of this effect,[1–3] a fully dynamic model accounting for the GMI response in a broad frequency range is still lacking.

Recently, a more general approach, based on the close relationship between the GMI effect and the ferromagnetic resonance (FMR), has been proposed.[4] It was shown that the calculation of GMI and FMR response are strictly equivalent, so that the simultaneous solution of Maxwell's equations and the Landau–Lifshitz equation could provide a rigorous theoretical framework to explain the GMI effect. To investigate this possibility, reliable high frequency data on GMI were required.

However, the frequency range of most of the early experiments, using conventional techniques such as oscilloscopes or impedance analyzers, was limited to about 100 MHz due to electromagnetic effect such as radiation, irregular propagation and impedance matching problems.[1–3,5] The experimental technique presented in this work was designed to overcome these difficulties and extend the measurements to the microwave range.[6–8]

Soft amorphous $Ni_{45}Co_{25}Fe_6Si_9B_{13}Mn_2$, $Co_{71}Fe_4Si_{14.5}Nb_4B_{6.5}$, and $Fe_{75}Si_{10}B_{15}$ fibers were cast by melt extraction.[9] The fibers, 30–40 μm in diameter, with resistivities of about 140 $\mu\Omega$ cm, were extracted directly from the melt by a sharp rotating wheel. During the cooling, strong tensile stresses were quenched-in, strongly affecting the fiber magnetic properties.[10]

The impedance of the fibers was measured from 1 kHz to 13 MHz using an HP4192A impedance analyzer in a standard four-probe configuration. The 18-mm-long fibers were placed within a Helmholtz coil pair, which supplies a maximum axial dc magnetic field of 120 Oe. The 15 μA (rms) drive current produced an alternating circumferential magnetic field with a maximum amplitude of 2 mOe at the surface of the fiber. In this range of currents, the GMI effect is linear, so we can use the standard definition for the impedance $Z = U/I$, where U is the voltage drop across the fiber and I is the amplitude of the drive current. All data were collected at room temperature, with the axes of the fibers normal to the earth's magnetic field.

The second measuring technique employed a coaxial transmission line in which a 7-mm-long fiber replaced the inner conductor (Fig. 1). The reflection coefficient of this line was measured up to 1.2 GHz with a network analyzer. The matching transition, inserted between the original inner conductor and one end of the fiber, is designed to suppress unwanted waveguide propagation modes. The other end of the fiber is attached to a short circuit piston. The power level of the driving signal was low enough to maintain the current through the fiber at less than 10 μA in amplitude, in order to avoid nonlinear effects as discussed above.

In the first setup, the electric field was directed axially with respect to the fiber, and the ac magnetic field generated by the drive current was circumferential. In the second setup, the transverse electromagnetic (TEM) mode of propagation in the coaxial segment is characterized by a radial transverse electric field, while the magnetic field component is still circumferential. Thus, the interaction of the fiber with the dc axially applied magnetic field is the same in both techniques.

The input impedance of the shorted line,

$$Z_{\mathrm{in}} = 50\,\frac{1+\Gamma}{1-\Gamma}, \tag{1}$$

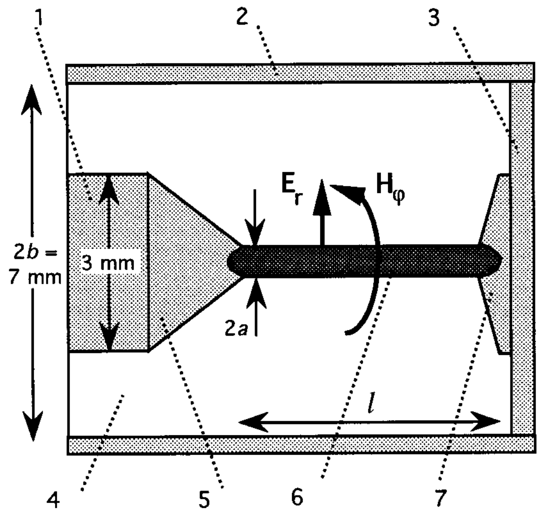

FIG. 1. Longitudinal cross-section of the coaxial line used to measure the GMI effect from 1 MHz to 1.2 GHz: (1) inner conductor, (2) outer conductor, (3) short-circuit piston, (4) air, (5) matching transition (conductor), (6) magnetic fiber, (7) conductor. Propagation modes and spatial distribution of the field components are also shown.

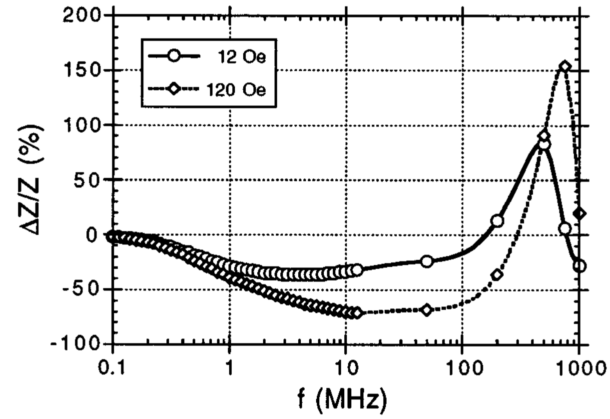

FIG. 2. GMI spectra of a NiCo-rich fiber for two dc axial magnetic fields. Data from 1 kHz to 13 MHz have been obtained with an impedancemeter. Data from 5 MHz to 1.2 GHz have been obtained with an impedance analyzer, using the setup in Fig. 1. In the latter case, the spectra have been plotted using a cubic spline curve fit.

was determined from the measured values of the reflection coefficient, Γ. Here, 50 stands for the characteristic impedance of an ideal line (50 Ω). In the case of a coaxial segment terminated with a short circuit, transmission line theory yields:[11]

$$Z_{\text{in}}=Z_c \tanh \gamma l, \tag{2}$$

where Z_c is the characteristic impedance, γ is the complex propagation constant, and l is the length of the line. Z_c and γ are often expressed in terms of the distributed circuit parameters and of the angular frequency ω of the propagating TEM mode as

$$Z_c=\sqrt{\frac{R+j\omega L}{G+j\omega C}} \quad \text{and} \quad \gamma=\sqrt{(R+j\omega L)(G+j\omega C)}, \tag{3}$$

where R and L are the distributed series resistance and inductance, and G and C the distributed shunt conductance and capacitance, respectively. The resistivity of the amorphous fiber is much higher than that of the outer conductor, so R is mainly related to the resistance of the magnetic core. Since G and C depend only upon the properties of the dielectric between the line and the coaxial shield (which is air in our case) and the geometry of the line, the impedance of the magnetic core is given by:

$$Z=R+j\omega L=Z_c\gamma, \tag{4}$$

where $L=L_i+L_e$ takes account of the internal and external components of the distributed inductance. In the high frequency range, where the skin depth δ is small compared to the dimension of the conductors, the impedance of the fiber is given by the simple expression:[11]

$$Z=\frac{R_S}{2\pi a}(1+j)+j\omega L_e, \tag{5}$$

where $R_S=1/(\sigma\delta)$ is the surface resistivity in Ω per square, $L_e=\mu_0 \ln(b/a)/2\pi$ is the line inductance in air, a and b are the inner and outer radius of the coaxial segment, σ is the electrical conductivity, μ is the effective permeability, and $\delta=\sqrt{2/\omega\mu\sigma}$ is the effective skin depth. In air, G is much smaller than ωC, where $C=2\pi\epsilon_0/\ln(b/a)$, and can be neglected. Therefore, substitution of Eqs. (4) and (5) in (3) yields:

$$Z_c=\frac{-jc^2\gamma L_e}{\omega}, \tag{6}$$

where c is the velocity of light. Substitution of Eq. (6) in (2) allows us to calculate Z_c and γ from Z_{in}. We then use (4) to solve for the impedance of the sample.

The impedance has been determined exactly using the Maxwell's equations and appropriate boundary conditions for the experimental geometry shown in Fig. 1.[8] A perturbation expansion of this solution yielded Eq. (6), showing that the approximations we have introduced here are justified.

At 1.2 GHz and below, the condition $l<\lambda/4$ is satisfied, so that the argument of the tangent in Eq. (2) is small and we can write $Z_{\text{in}}\cong Z_c\gamma l=Zl$. Thus, the impedance of the fiber is well approximated by the input impedance per unit length of the shorted line. These results, obtained from 5 MHz to 1.2 GHz, were compared to those measured from 1 kHz to 13 MHz with the impedance analyzer. Reasonable agreement between the two techniques was observed between 5 and 13 MHz, where their frequency ranges overlap.

The giant magnetoimpedance effect, which is defined as

$$\frac{\Delta Z}{Z}=\frac{|Z(H)|-|Z(H_{\text{ref}})|}{|Z(H_{\text{ref}})|},$$

where $H_{\text{ref}}=0$, is shown in Fig. 2 as a function of the frequency for two dc applied fields for a NiCo-rich amorphous fiber. In the low frequency range ($f<100$ MHz), the effect is negative and shows a maximum of -70% at 30–40 MHz for $H=120$ Oe, as reported earlier.[5] At higher frequency, a tran-

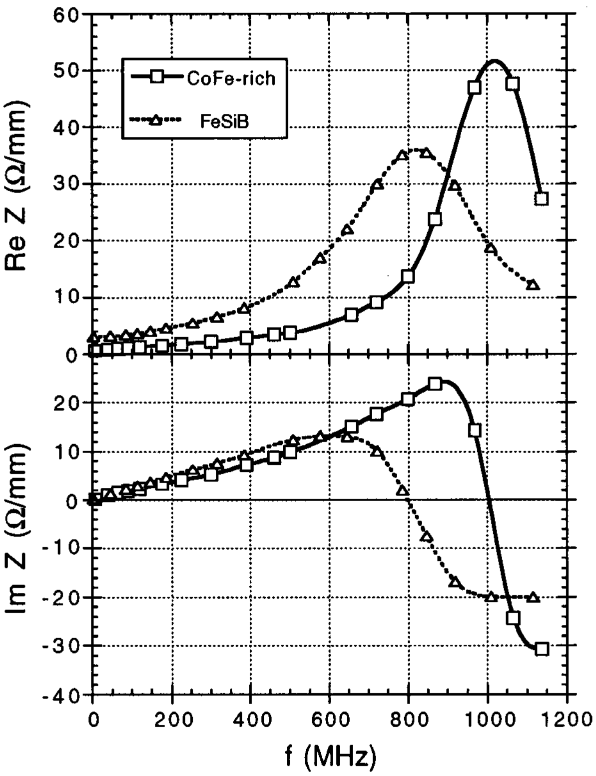

FIG. 3. Real and imaginary parts of the impedance of CoFe-rich and FeSiB fibers as functions of the frequency. The applied field was 120 Oe. Re Z peaks and Im Z crosses zero at the same frequency for each fiber. Cubic spline fitting was used again.

sition of the effect from negative to positive occurs. The GMI ratio then reaches a maximum, peaking at higher frequency for higher fields. This trend suggests the occurrence of a resonance.

According to Eq. (5), the intrinsic impedance of the fiber, $Z_i = R + j\omega L_i = Z - j\omega L_e$, varies as $Z_i \propto \sqrt{j\omega\mu(H,\omega)}$. The theoretical dependence of the effective permeability, $\mu = \mu' - j\mu''$, with frequency, shows around the resonance a characteristic peak for μ'', while μ' crosses zero.[12] This results in resonant behavior for the real and imaginary parts of the intrinsic impedance: the real part peaks as the imaginary part crosses zero. We verified this trend experimentally for all our fibers, as shown in Fig. 3. For an 120 Oe applied field, the resonance frequency is about 800 MHz for FeSiB and 1000 MHz for CoFe-rich fibers.

The GMI responses of a NiCo-rich amorphous fiber for several frequencies, are plotted in Fig. 4 as functions of the dc field strength. The general appearance of the response shows positive peaks at low field, followed by negative dependences saturating at high field. Depending on frequency, one or the other of these features will dominate. In the 1–10 MHz range, the positive peaks are small (only 4% at 10 MHz), and the response is predominantly negative, reaching −70% at saturation. Between 10 and 100 MHz, a mixed response showing moderate peaks and negative saturation values is observed. Over 100 MHz, the response becomes predominant positive, with large peaks (about 70% at 500 MHz), which are displaced toward higher field (40 Oe at 500 MHz). These peaks may be viewed as another indication of a resonance occurring in the system.

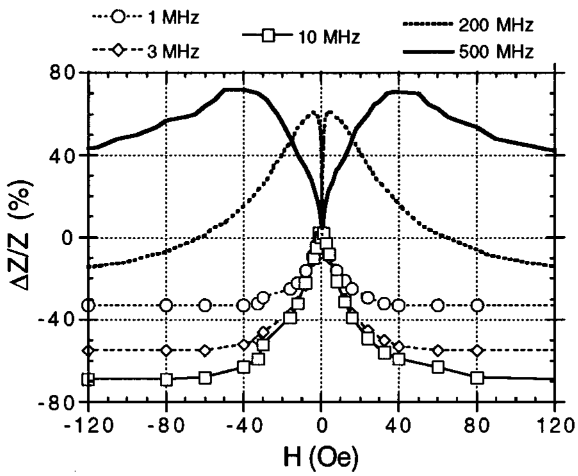

FIG. 4. GMI responses of a NiCo-rich fiber for frequencies ranging from 1 MHz to 500 MHz.

High frequency impedance spectra provided useful information for modeling the GMI effect. We have shown that the experimental results are in agreement with the relationship we propose between GMI and FMR responses. Many questions regarding the application of the FMR theoretical framework to the GMI effect remain open, especially in the low frequency range, at low field or high driving currents, where the effect is nonlinear. Future work will have to consider the possible effect of stress-induced anisotropy and domain structure on resonance. High frequency GMI shows great possibilities for such applications as magnetic field-controlled microwave devices, and holds the potential for becoming a technique for characterizing magnetic materials.

This work was supported by grants from FCAR (Quebec) and NSERC (Canada).

[1] L. V. Panina, K. Mohri, T. Uchiyama, M. Noda, and K. Bushida, IEEE Trans. Magn. **31**, 1249 (1995).
[2] R. S. Beach, N. Smith, C. L. Platt, F. Jeffers, and A. E. Berkowitz, Appl. Phys. Lett. **68**, 2753 (1996).
[3] F. L. A. Machado and S. M. Rezende, J. Appl. Phys. **79**, 6558 (1996).
[4] A. Yelon, D. Ménard, M. Britel, and P. Ciureanu, Appl. Phys. Lett. **69**, 3084 (1996).
[5] P. Ciureanu, P. Rudkowski, G. Rudkowska, D. Ménard, M. Britel, J. F. Currie, J. O. Ström-Olsen, and A. Yelon, J. Appl. Phys. **79**, 5136 (1996).
[6] M. Britel, D. Ménard, P. Ciureanu, C. Akyel, J. Gauthier, and A. Yelon, Proceedings of the Symposium on Antenna Technology and Applied Electromagnetics, Montreal, 1996, p. 823.
[7] P. Ciureanu, C. Akyel, M. Britel, J. Gauthier, A. Yelon, P. Rudkowski, G. Rudkowska, and J. O. Ström-Olsen, IEEE Trans. Magn. **32**, 4678 (1996).
[8] V. P. Paramonov and A. S. Antonov (unpublished).
[9] P. Rudkowski and J. O. Ström-Olsen, U.S. Patent 5,003,291 (1991).
[10] P. Ciureanu, G. Rudkowska, P. Rudkowski, and J. O. Ström-Olsen, IEEE Trans. Magn. **29**, 2251 (1993).
[11] R. A. Chipman, *Transmission Lines* (McGraw-Hill, New York, 1968).
[12] S. Chikazumi, *Physics of Magnetism* (Wiley, New York, 1964).